Geochemistry, Geophysics, Geosystems

Supporting Information for

Geochemical and geophysical constrains on the dynamic topography of the Southern African Plateau

Alan G. Jones[1,2,4], Juan Carlos Afonso[2,3], Javier Fullea[4]

1 Complete MT Solutions, Ottawa, Ontario, Canada

2 Macquarie University, Sydney, NSW, Australia

3 Centre for Earth Evolution and Dynamics (CEED), University of Oslo, Norway.

4 Dublin Institute for Advanced Studies, Dublin 2, Ireland

Contents of this file

Introduction

This Supporting Information contains a note about computation time and figures related to four of the five tests reported in the main text.

Computation times

All computations for Tests 1-4 were performed serially on a Mac Mini with an Intel i5 processor running at 2.8 GHz taking of the order of 1 min for 1,000 candidate models. The computations for Test 5 involved 10 concurrent runs of 30 million candidate models each, and were performed on a 2x6-core Intel 3.33 GHz Intel Xeon X5680 CPUs at DIAS, taking of the order of 1 min for 1,500 candidate models.

Test 2 Figures - Inversion of Rayleigh wave data with general oxide geochemistry constraints

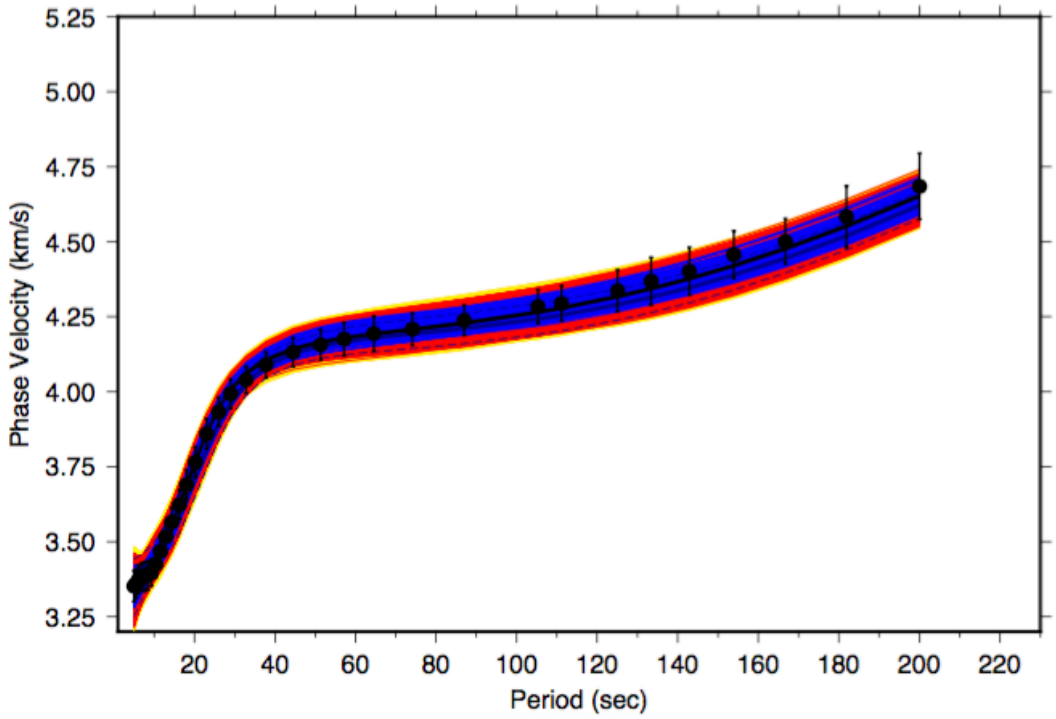

Figure S1.2.1A: Fits of the models to the Rayleigh wave dispersion data with imposed geochemistry constraints for the lithospheric and sub-lithospheric mantle. Yellow (hidden beneath the red and blue models) denotes models with a normalized root mean square (nRMS) ≤1, red nRMS≤0.89, and blue nRMS≤0.60.

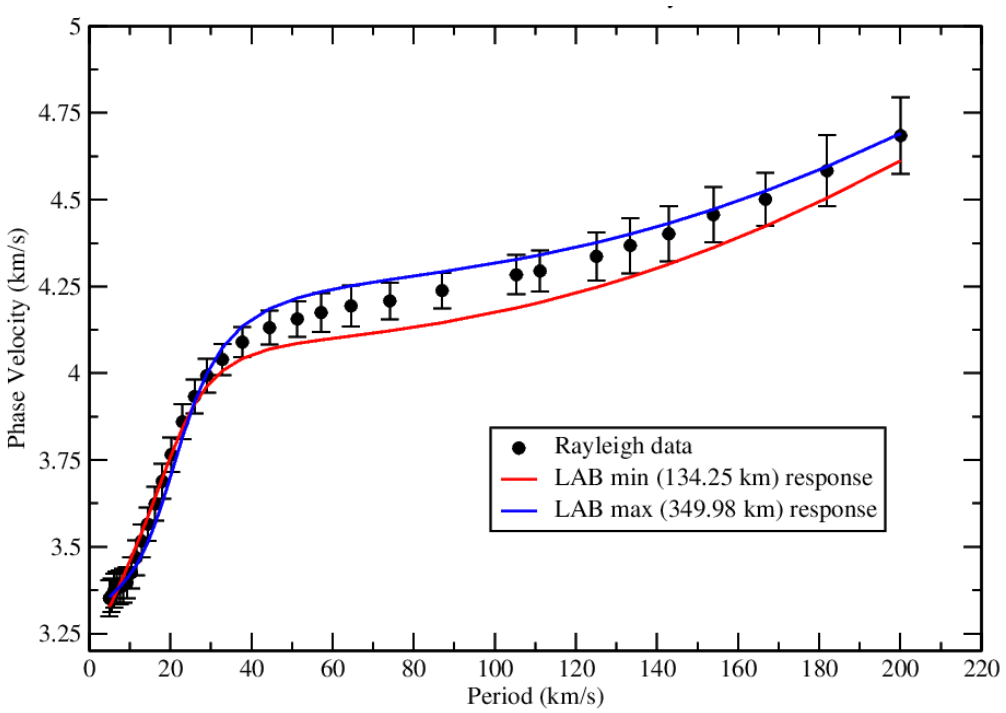

Figure S1.2.1A: Fits of the two extremal models that fit to nRMS≤1 with the minimum LAB (red curve) and the maximum LAB (blue curve) of 134.25 and 349.98 km respectively. Note that the red bound, although it fits to within an nRMS<1.00, would be considered unacceptable when serial correlations of residuals is taken into consideration.

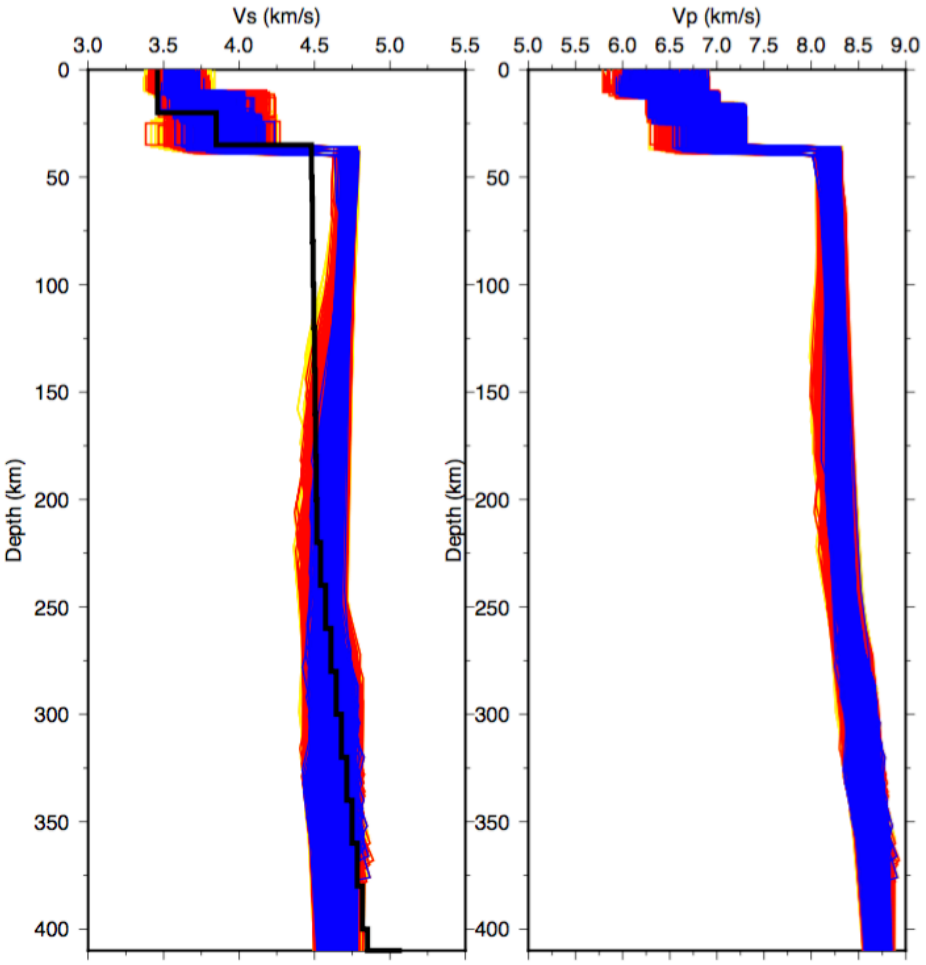

Figure SI2.2: Seismic Vs (left) and Vp models acceptable to the data (Fig. SI2.1A). Yellow denotes models with an nRMS≤1, red nRMS≤0.89, and blue nRMS≤0.60. Also shown on the Vs models plot is the AK135 global model of *Kennett et al.* [1995].

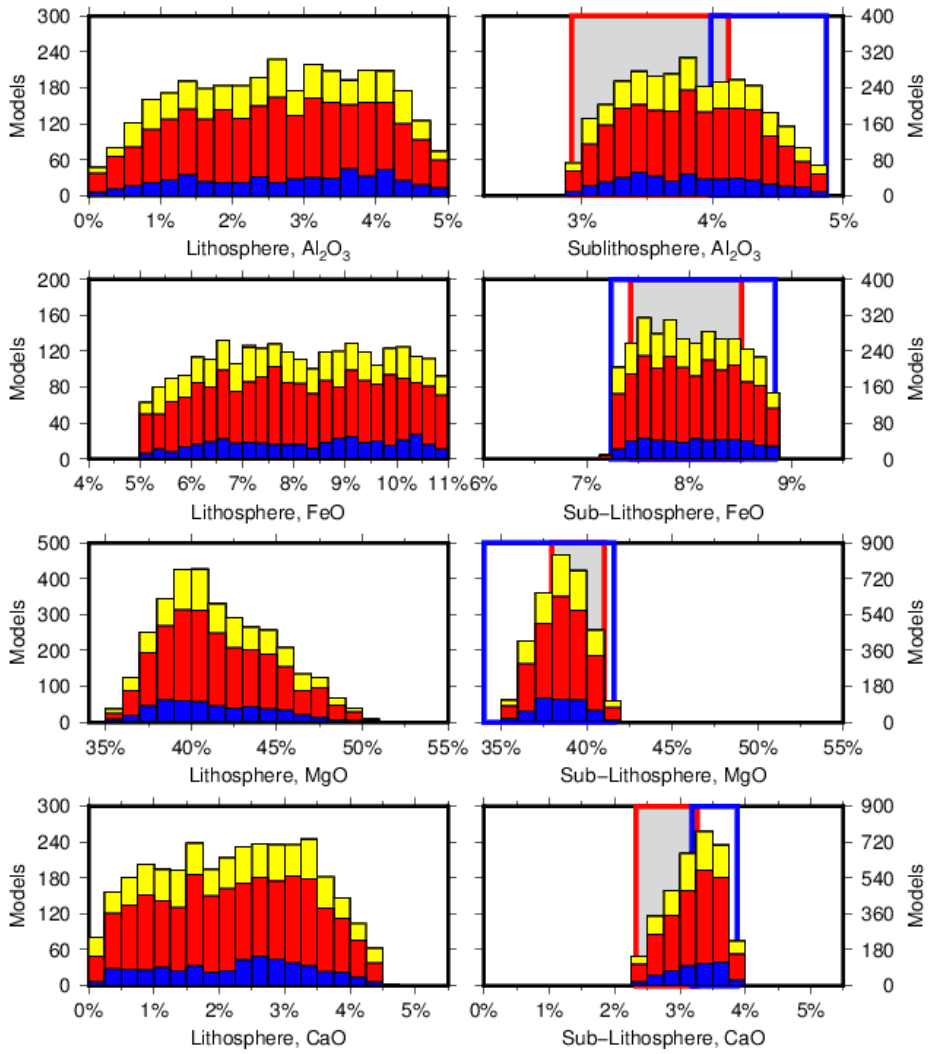

Figure S12.3: Posterior PDFs of the oxide chemistries of the lithospheric layer (column 1) and the sub-lithospheric mantle (column 2). The four rows are respectively percentages of Al_2O_3, FeO, MgO and CaO; the fifth oxide, SiO_3, is 100% minus the sum of all four. The two boxes on the SLM oxides are the Primitive Upper Mantle ranges for *McDonough and Sun* [1995] (blue boxes) and *Lyubetskaya and Korenaga* [2007] (grey shaded red boxes). All models were chosen from prior PDFs that sampled the globally-observed oxide database (Table 3, main text). Yellow denotes models with an nRMS≤1, red nRMS≤0.93, and blue nRMS≤0.60.

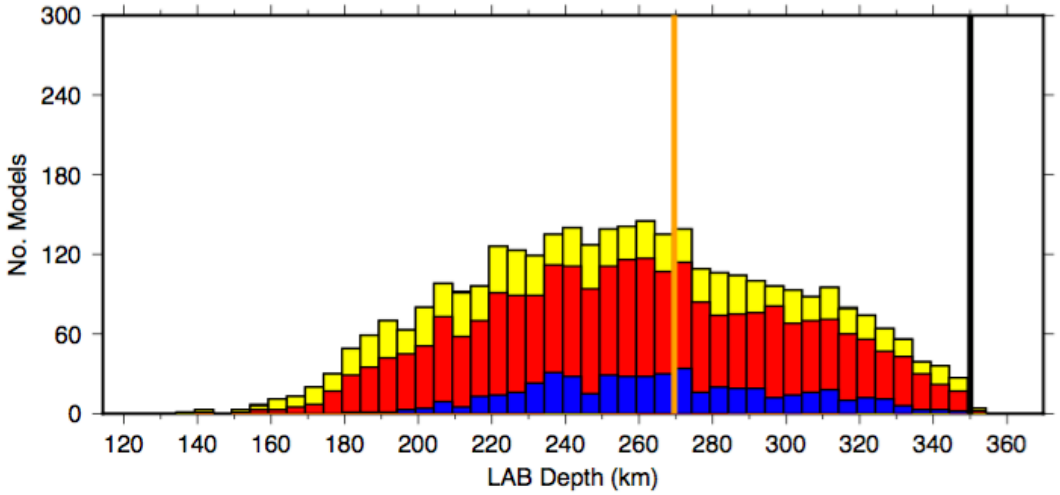

Figure S12.4: Posterior PDF of the LAB depths of the successful models with constrained oxide geochemistry. Yellow denotes models with an nRMS≤1, red nRMS≤0.89, and blue nRMS≤0.60. The thick vertical black line denotes the upper bound imposed (lower bound of 100 km not plotted), and the thick vertical orange line denotes the LAB for the best-fitting model.

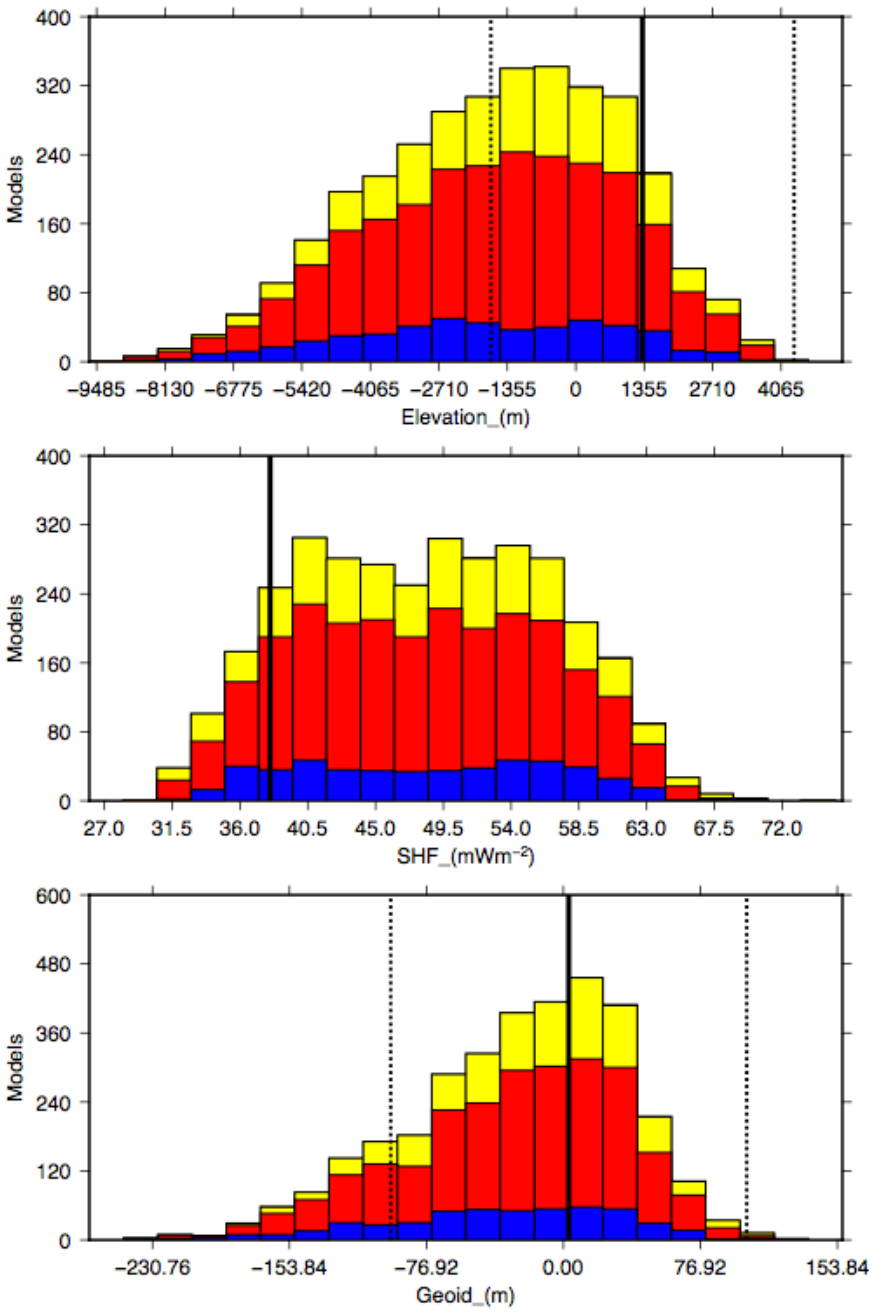

Figure S12.5: Posterior PDFs of the elevation (top), surface heat flow (middle) and geoid height (bottom) for the successful models fit only to the Rayleigh data with oxide geochemistry constraints on the lithospheric and sub-lithospheric mantle. Yellow denotes models with an nRMS≤1, red an nRMS≤0.89, and blue an nRMS≤0.60. The solid vertical black lines are the actual observations. The standard errors (denoted by dashed vertical black lines) are greatly expanded to allow prior PDFs a very large range.

Test 3 Figures - Inversion of Rayleigh wave data, reduced geoid height and surface heat flow data with general oxide geochemistry constraints

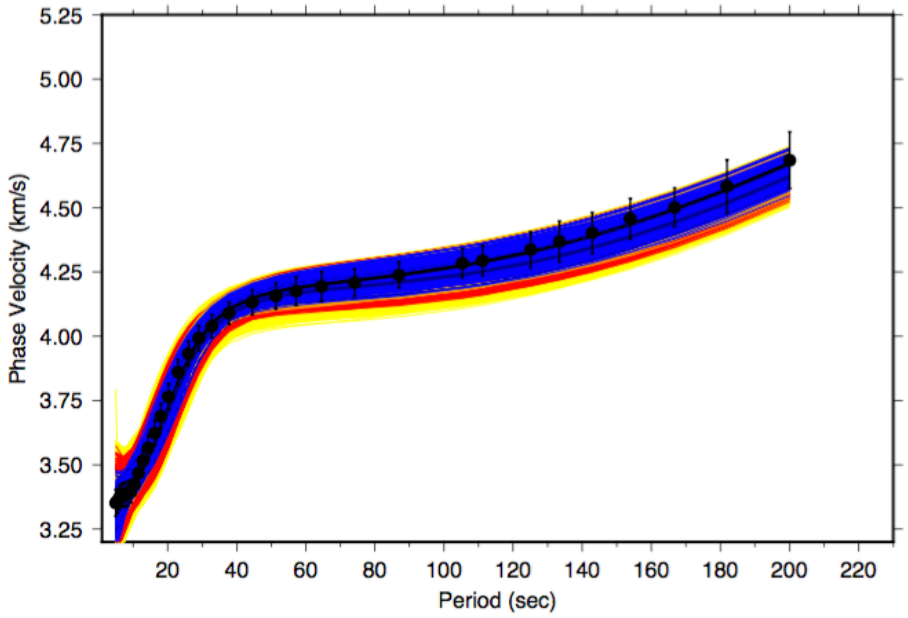

Figure S13.1A: Fits of the models to the Rayleigh wave dispersion data, SHF and elevation with imposed geochemistry constraints for the lithospheric and sub-lithospheric mantle. Yellow denotes models with an nRMS≤1, red nRMS≤0.66, and blue nRMS≤0.46. Gold denotes models that fit all three data types each to an RMS or nRMS≤1.

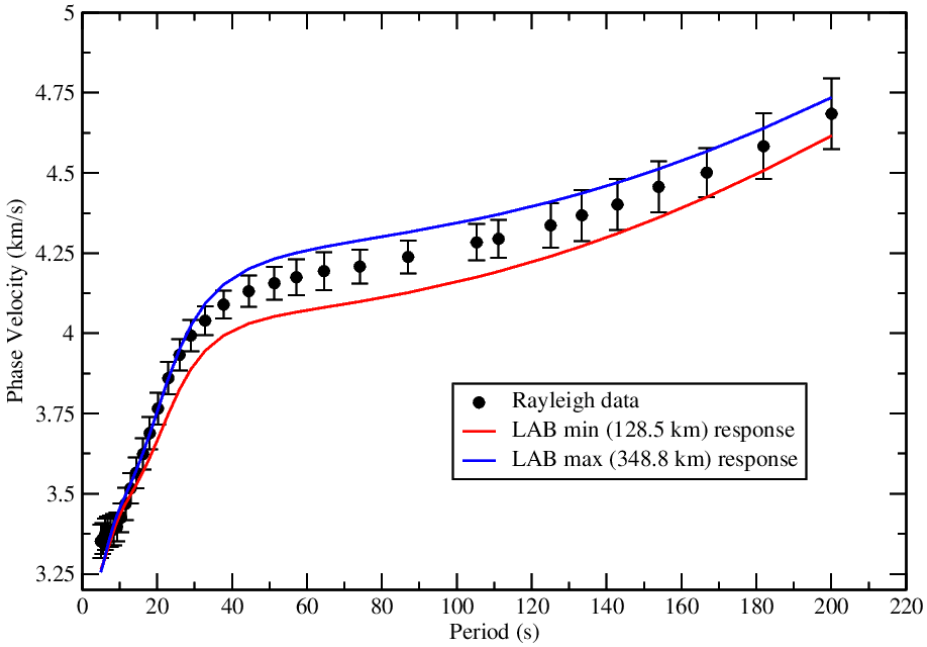

Figure S13.1B: Fits of the two extremal models that fit to nRMS≤1 with the minimum LAB (red curve) and the maximum LAB (blue curve) of 128.5 and 348.8 km

respectively. Note that these extreme bounds would be considered statistically unacceptable models when serial correlations of residuals is considered, and therefore realistic models lie well inside these bounds (see Fig. SM3.4).

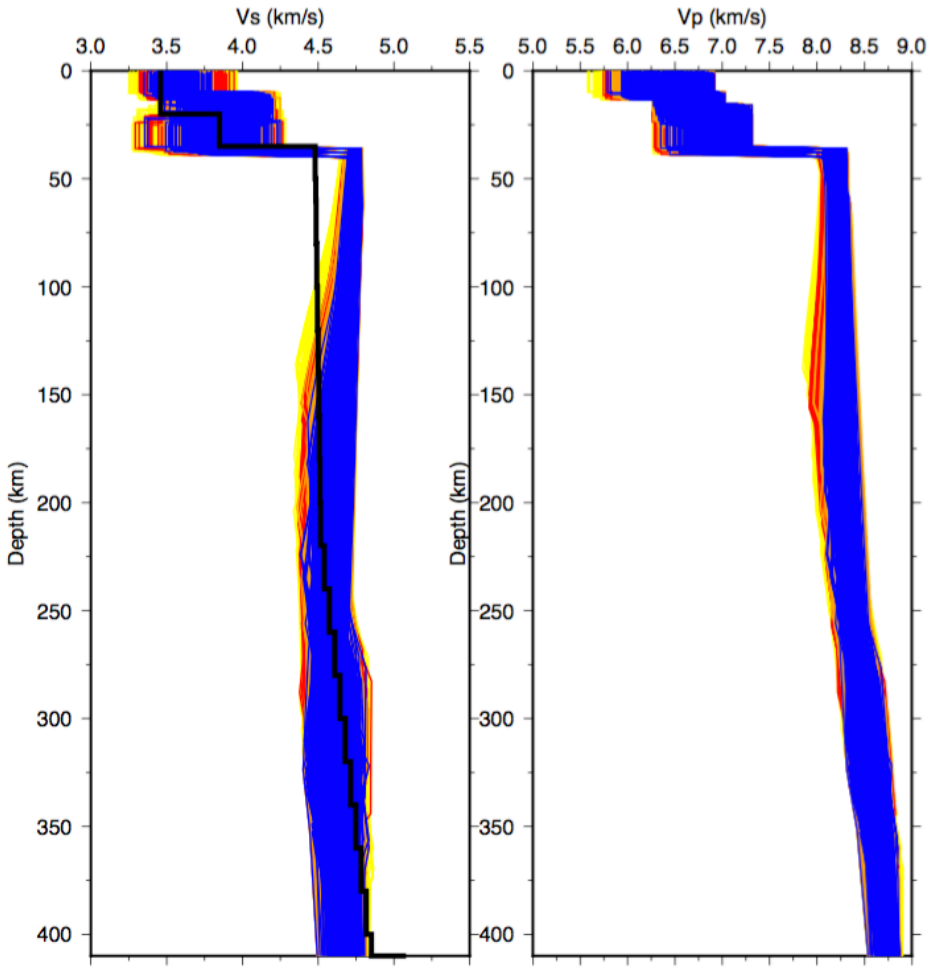

Figure SI3.2: Seismic Vs (left) and Vp models acceptable to the data (Fig. SI3.1A). Yellow denotes models with an nRMS≤1, red nRMS≤0.66, and blue nRMS≤0.46. Gold denotes models that fit all three data types each to an RMS or nRMS≤1. Also shown on the Vs models plot is the AK135 global model of *Kennett et al.* [1995].

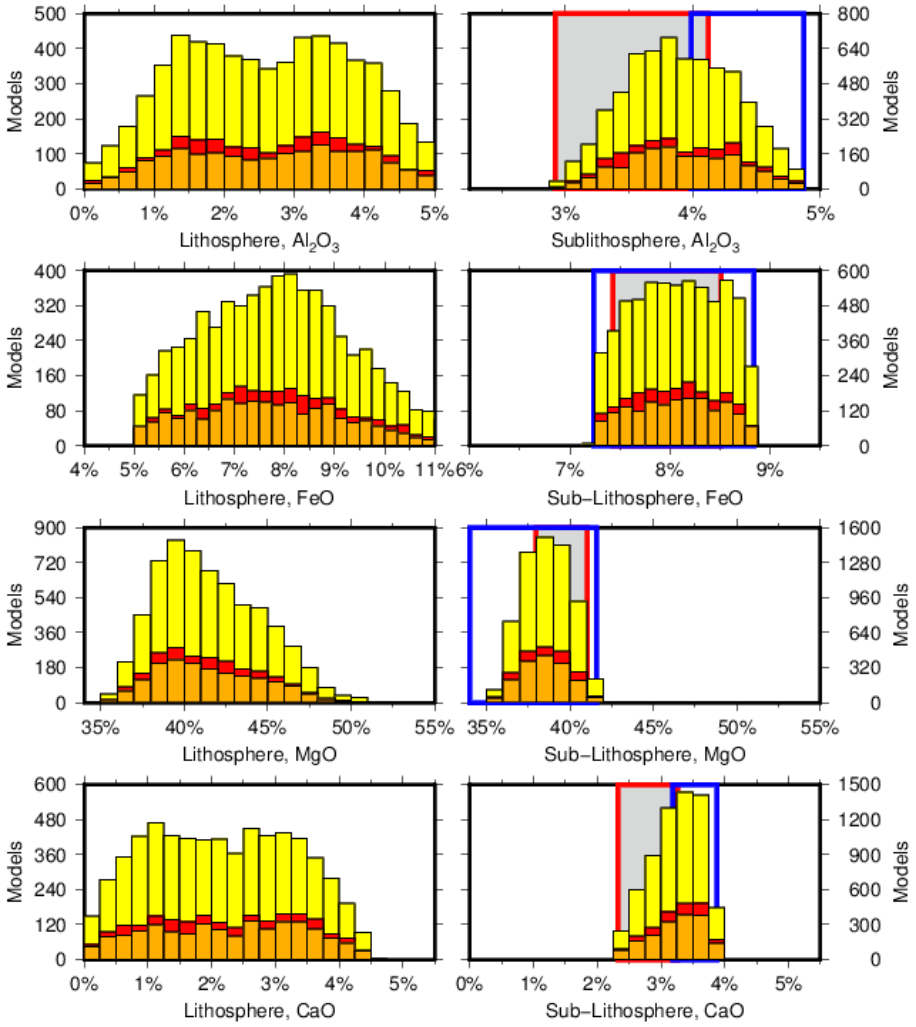

Figure S13.3: Posterior PDFs of the oxide chemistries of the lithospheric layer (column 1) and the sub-lithospheric mantle (column 2). The four rows are respectively percentages of Al_2O_3, FeO, MgO and CaO; the fifth oxide, SiO_3, is 100% minus the sum of all four. The two boxes on the SLM oxides are the Primitive Upper Mantle ranges for *McDonough and Sun* [1995] (blue boxes) and *Lyubetskaya and Korenaga* [2007] (grey shaded red boxes). All models were chosen from prior PDFs that sampled the globally-observed oxide database (Table 3, main text). Yellow denotes models with an nRMS≤1, red nRMS≤0.66, and blue nRMS≤0.46. Gold denotes models that fit all three data types each to an RMS or nRMS≤1.

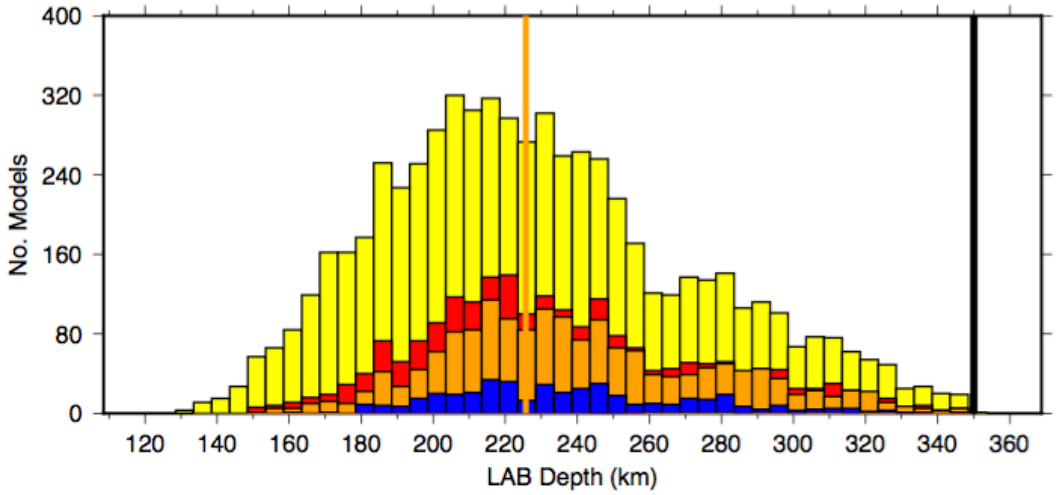

Figure S13.4: Posterior PDF of the LAB depths of the successful models with constrained oxide geochemistry. Yellow denotes models with an nRMS≤1, red nRMS≤0.66, and blue nRMS≤0.46. Gold denotes models that fit all three data types each to an RMS or nRMS≤1. The thick vertical black line denotes the upper bound imposed (lower bound of 100 km not plotted), and the thick vertical orange line denotes the LAB for the best-fitting model.

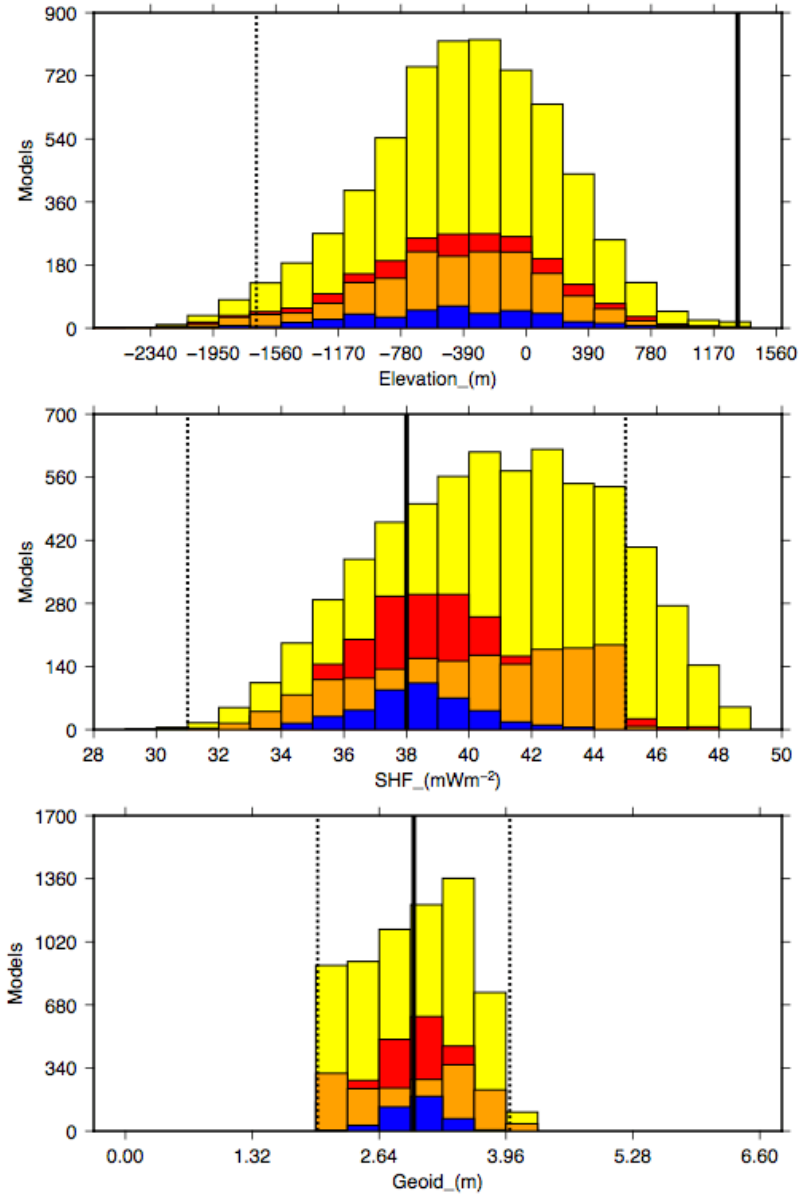

Figure S13.5: Posterior PDFs of the elevation (top), surface heat flow (middle) and geoid height (bottom) for the successful models fit to the Rayleigh, SHF and geoid data with oxide geochemistry constraints on the lithospheric and sub-lithospheric mantle. Yellow denotes models with an nRMS≤1, red nRMS≤0.66, and blue nRMS≤0.46. Gold denotes models that fit all three data types each to an RMS or nRMS≤1. The solid vertical black lines are the actual observations. The standard errors (denoted by dashed vertical black lines) are correct for SHF and geoid, but are greatly expanded to allow the prior PDF a very large range.

Test 4 Figures - Inversion of Rayleigh wave data, reduced geoid height and surface heat flow data plus MT data with general oxide geochemistry constraints

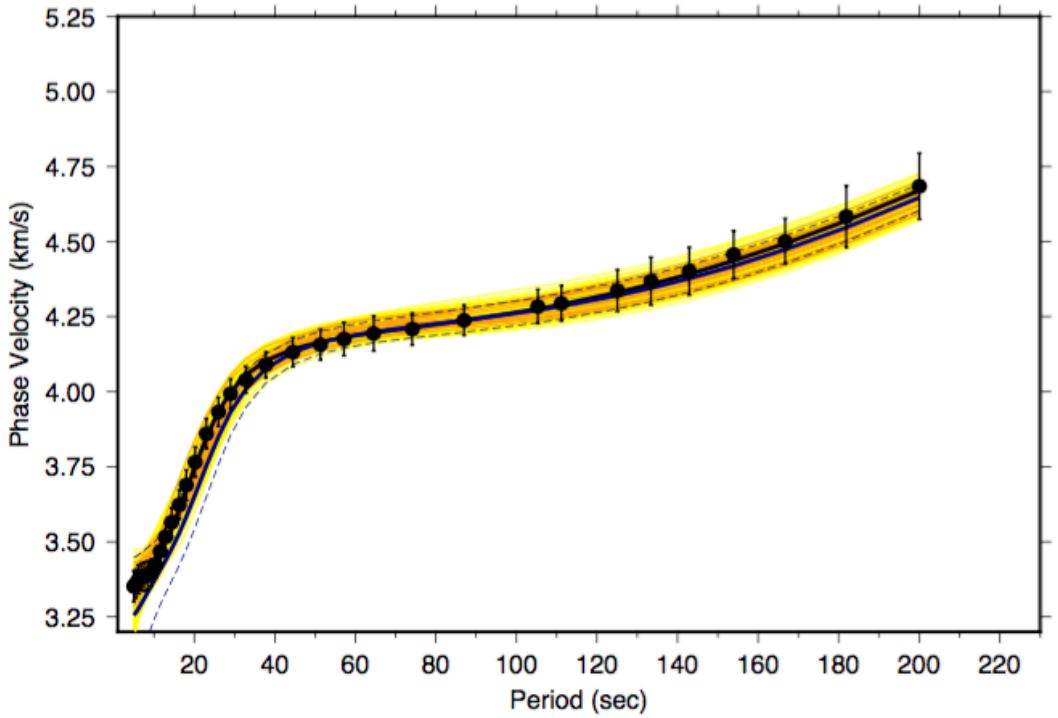

Figure S14.1A: Fits of the models to the Rayleigh wave dispersion data, SHF and elevation with imposed geochemistry constraints for the three lithospheric layers and the sub-lithospheric mantle. Yellow denotes models with an nRMS≤1, whereas gold denotes models that fit all three data types each to an RMS or nRMS≤1.

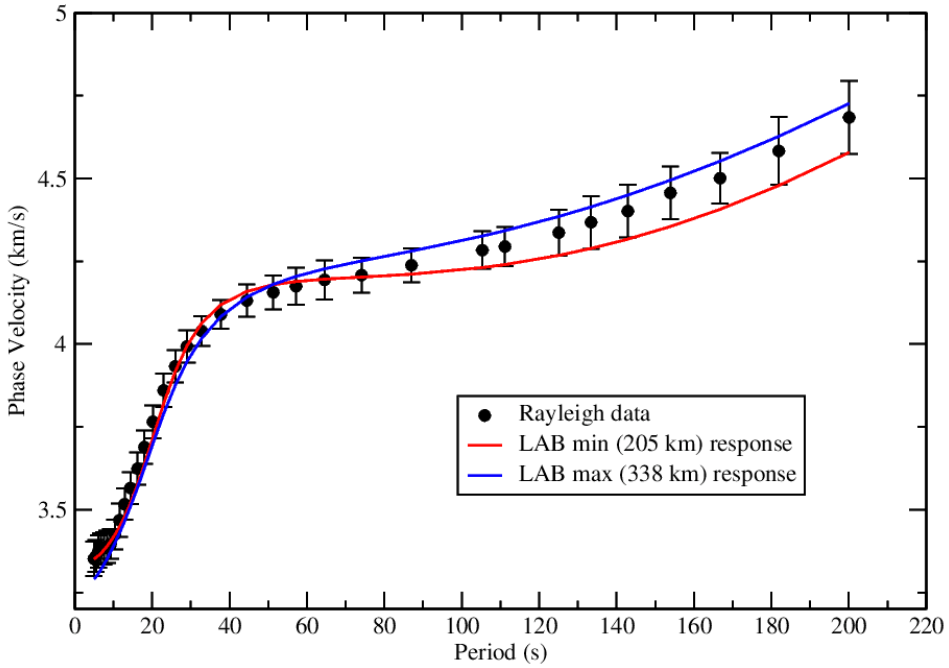

Figure S14.1B: Fits of the two extremal models that fit to nRMS≤1 with the minimum LAB (red curve) and the maximum LAB (blue curve) of 205 and 338 km respectively.

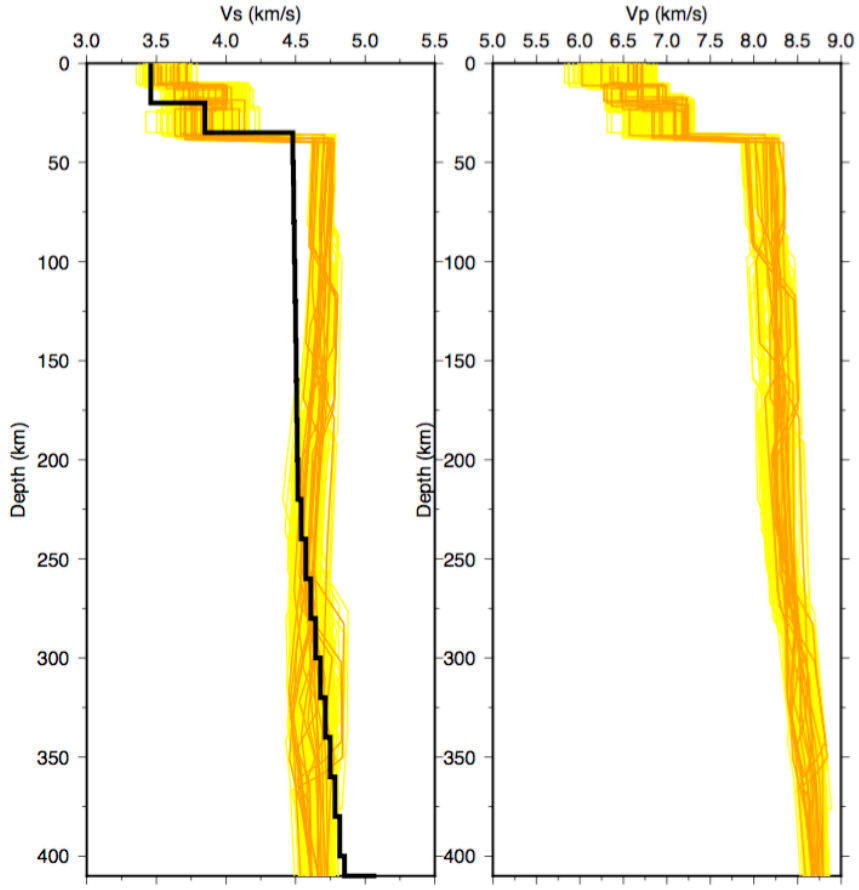

Figure S14.2: Seismic Vs (left) and Vp models acceptable to the data (Fig. SM4.1). Yellow denotes models with an nRMS≤1, and gold denotes models that fit all three data types each to an RMS or nRMS≤1. Also shown on the Vs models plot is the AK135 global model of *Kennett et al.* [1995].

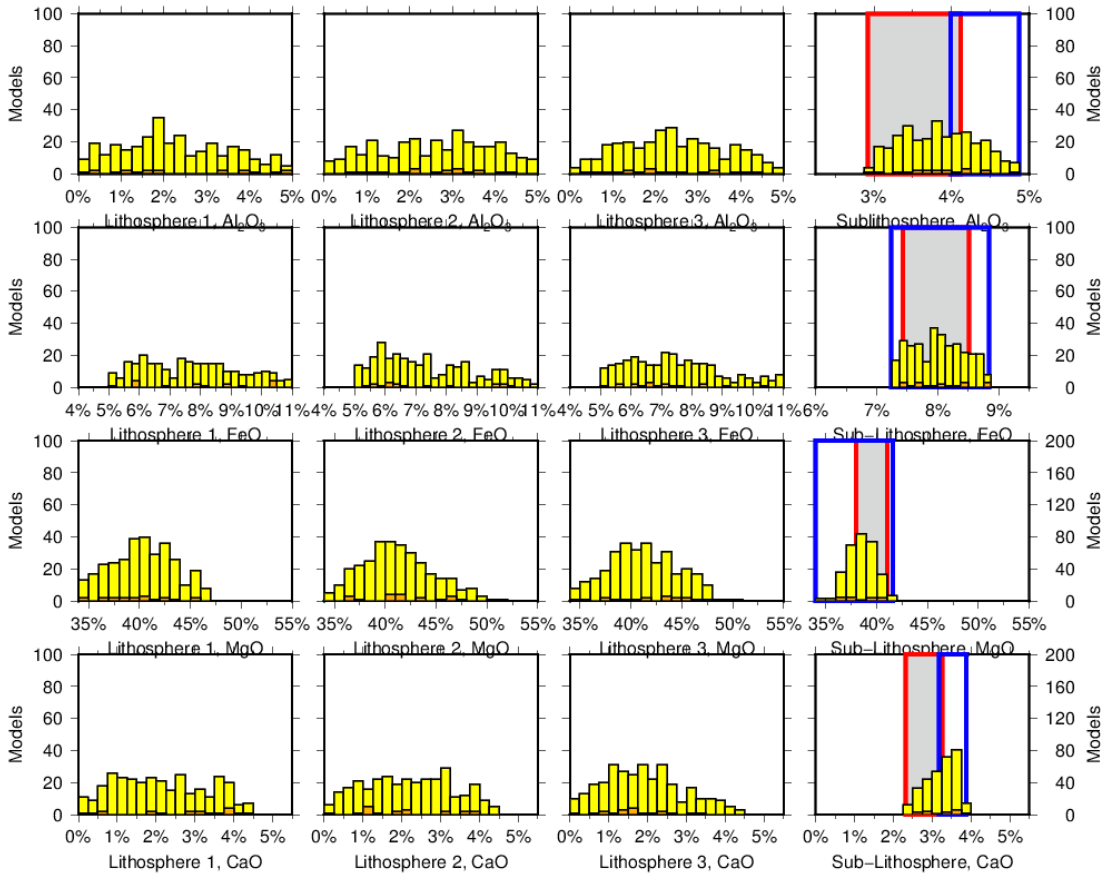

Figure S14.3: Posterior PDFs of the oxide chemistries of the three lithospheric layers (columns 1, 2 and 3 for layers 1, 2 and 3 respectively) and the sub-lithospheric mantle (column 4). The four rows are respectively percentages of Al_2O_3, FeO, MgO and CaO; the fifth oxide, SiO_3, is 100% minus the sum of all four. The two boxes on the SLM oxides are the Primitive Upper Mantle ranges for *McDonough and Sun* [1995] (blue boxes) and *Lyubetskaya and Korenaga* [2007] (grey shaded red boxes). All models were chosen from prior PDFs that sampled the globally-observed oxide database (Table 3, main text). Yellow denotes models with an nRMS≤1, and gold denotes models that fit all three data types each to an RMS or nRMS≤1.

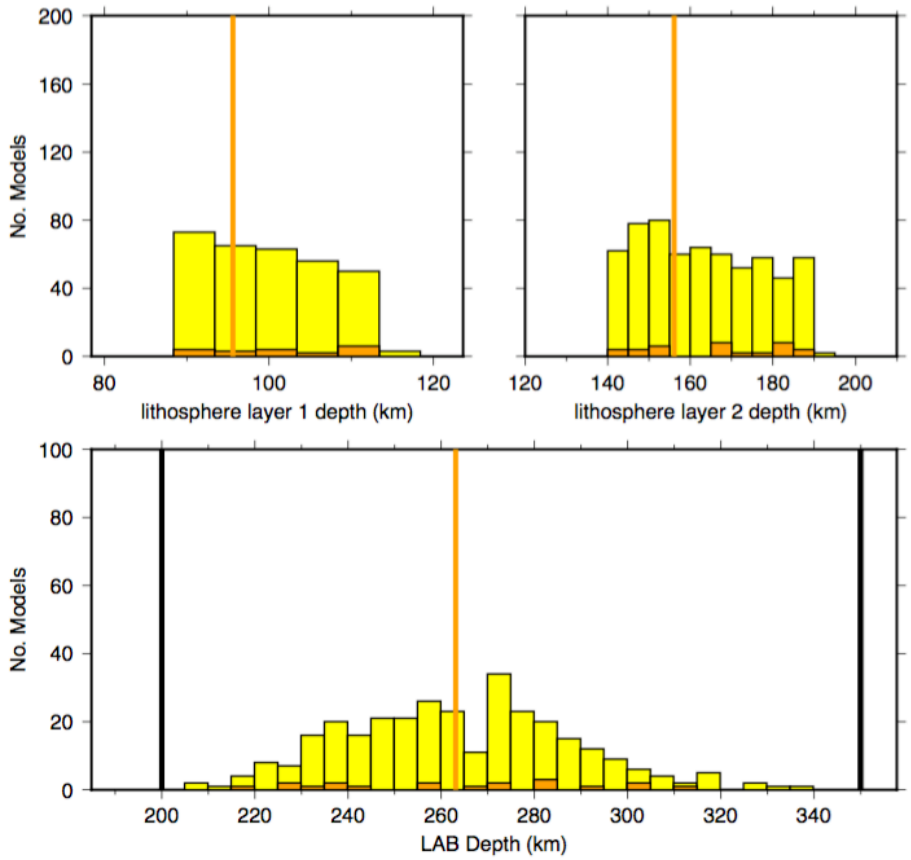

Figure S14.4: Posterior PDF of the LAB depths of the successful models with constrained oxide geochemistry. Yellow denotes models with an nRMS≤1, and gold denotes models that fit all three data types each to an RMS or nRMS≤1. The thick vertical black line denotes the bounds imposed, and the thick vertical orange lines denote the MLD1, MLD2 and the LAB for the best-fitting model.

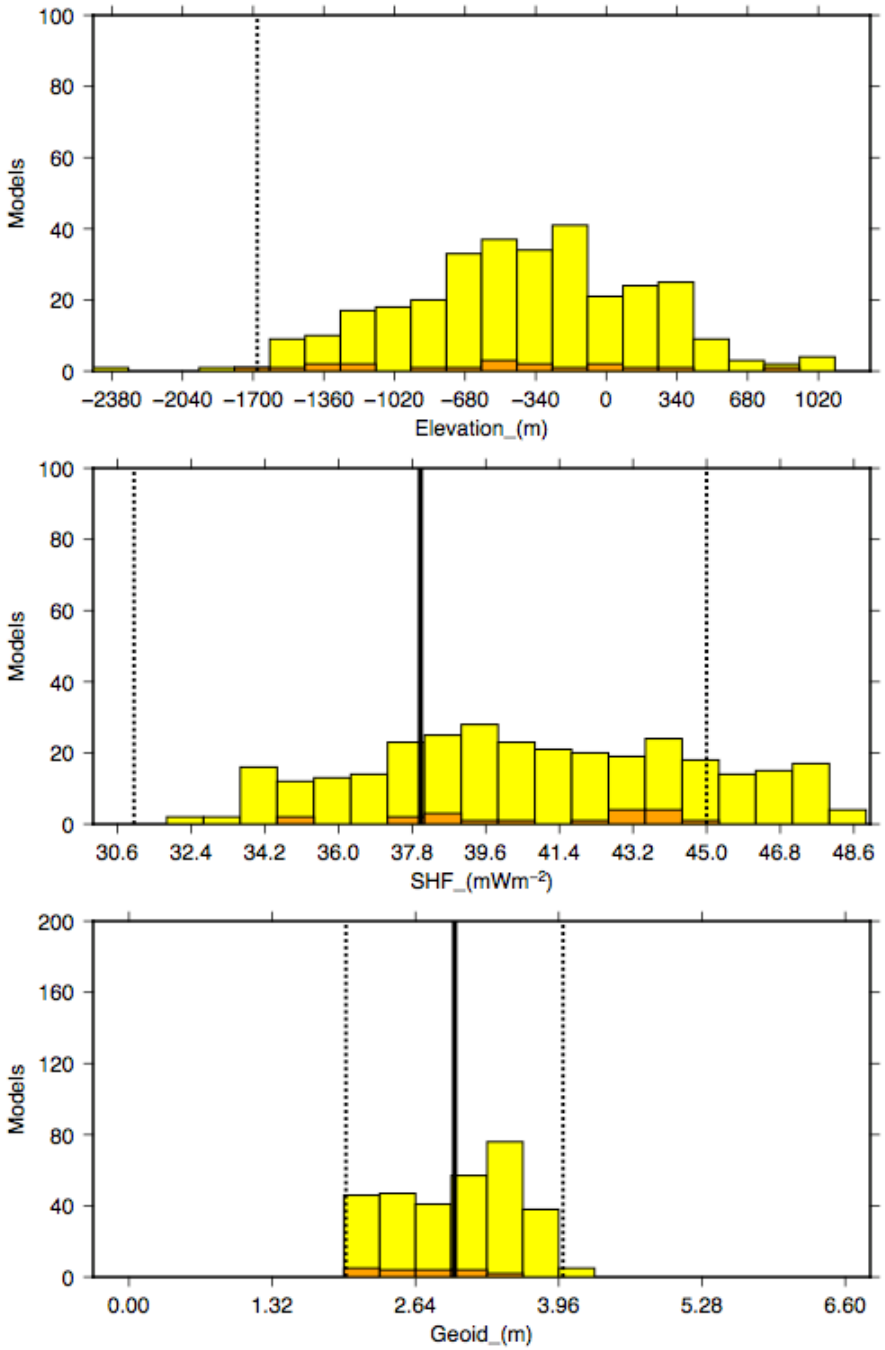

Figure S14.5: Posterior PDFs of the elevation (top), surface heat flow (middle) and geoid height (bottom) for the successful models fit to the Rayleigh, SHF and geoid data with oxide geochemistry constraints on the lithospheric and sub-lithospheric mantle. Yellow denotes models with an nRMS≤1, and gold denotes models that fit all three data types each to an RMS or nRMS≤1. The solid vertical black lines are the actual observations (not shown on the elevation plot). The standard errors (denoted by dashed vertical black lines) are correct for SHF and geoid, but are greatly expanded to allow the prior PDF a very large range.

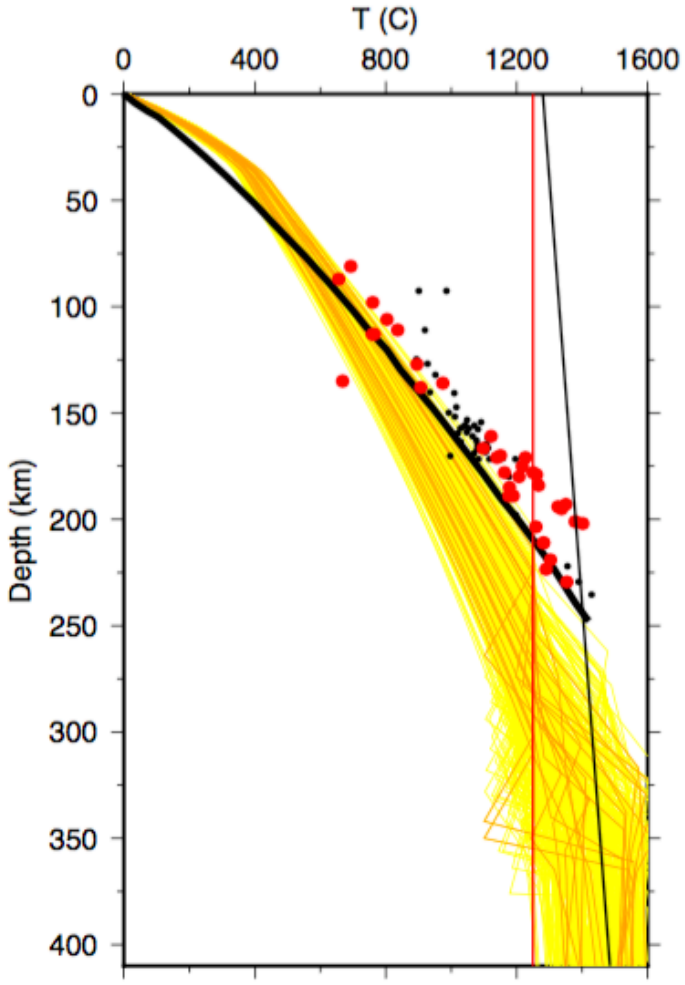

Figure S14.6: Geotherms for the successful models. Yellow denotes models with an nRMS < 1.00, and gold denotes those models that fit all four data types independently to an nRMS<1. Also plotted on the figure is geotherm K2 (solid thick black line) of the Kaapvaal Craton derived by *Jones* [1988] based on the heat flow from granitic terranes, and the petrologically-derived P-T data based on petrological geothermometry of xenoliths from the Group I kimberlites on the Kaapvaal Craton [*Woodland and Koch*, 2003] (red for Jagersfontein, black for other kimberlite fields). The solid thin black line is the peridotite melting adiabat of *McKenzie and Bickle* [1990], and the solid thin red line is 1250 °C, which is the assumed thermal LAB. The solid thin black line is the peridotite melting adiabat of *McKenzie and Bickle* [1988; 1990], and the solid thin red line is 1250 °C, which is the assumed thermal LAB.

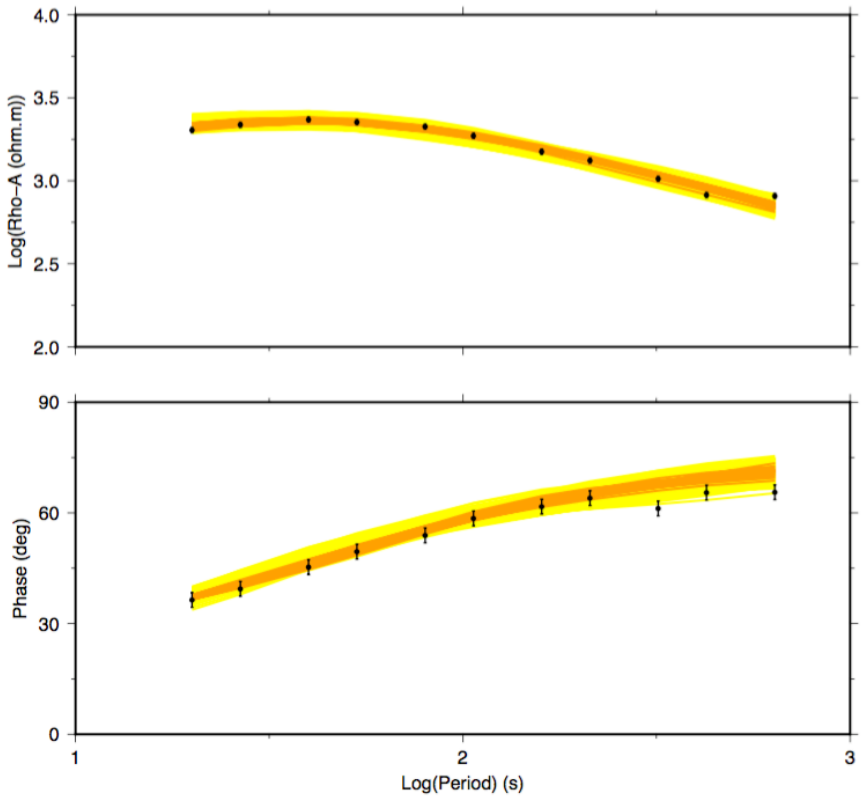

Figure S14.7: Fits of the models to the MT data (black circles with error bars). Yellow denotes models with an nRMS < 1.00, and gold denotes those models that fit all four data types independently to an nRMS<1.

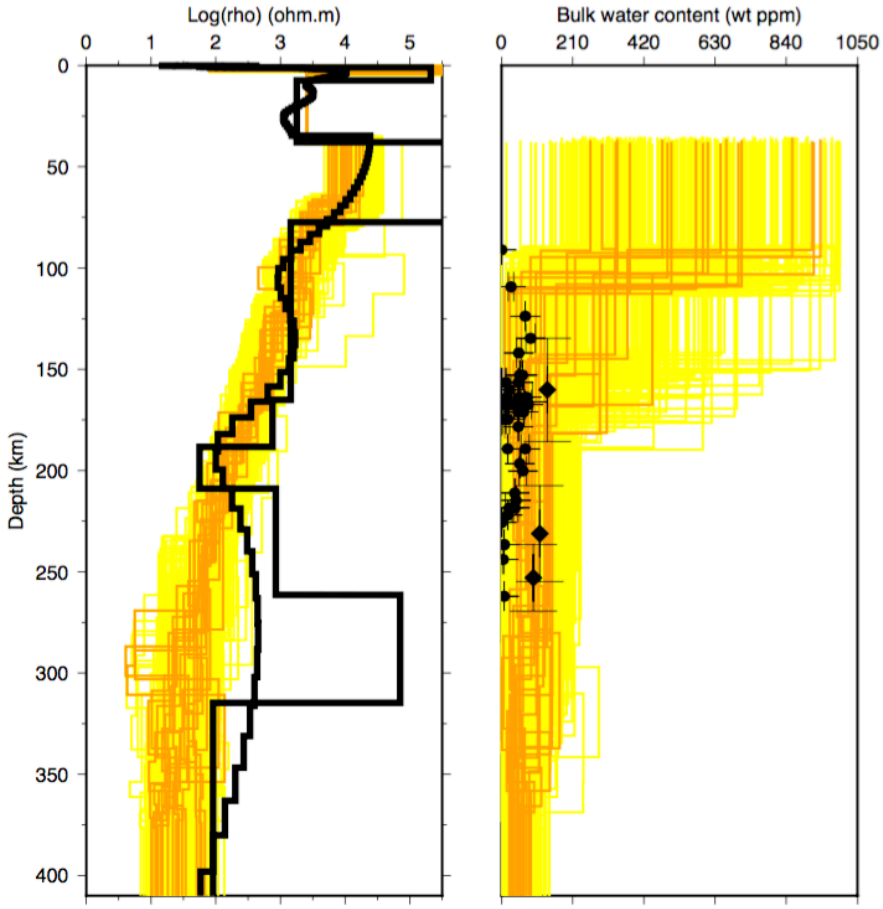

Figure S14.8: Electrical resistivity (left column) and bulk water content (right column) models. Yellow denotes models with an nRMS < 1.00, and gold denotes those models that fit all four data types independently to an nRMS<1. Also shown on the resistivity models plot are the best-fitting layered Earth models and best-fitting Occam smooth model (black lines), and on the water models plot are the bulk water and water in olivine contents from *Peslier et al.* [2010] as black symbols with error bounds.

Test 5 Figures - Inversion of Rayleigh wave data, reduced geoid height and surface heat flow data plus MT data with layer-specific oxide geochemistry constraints and consistent with geotherm and water content

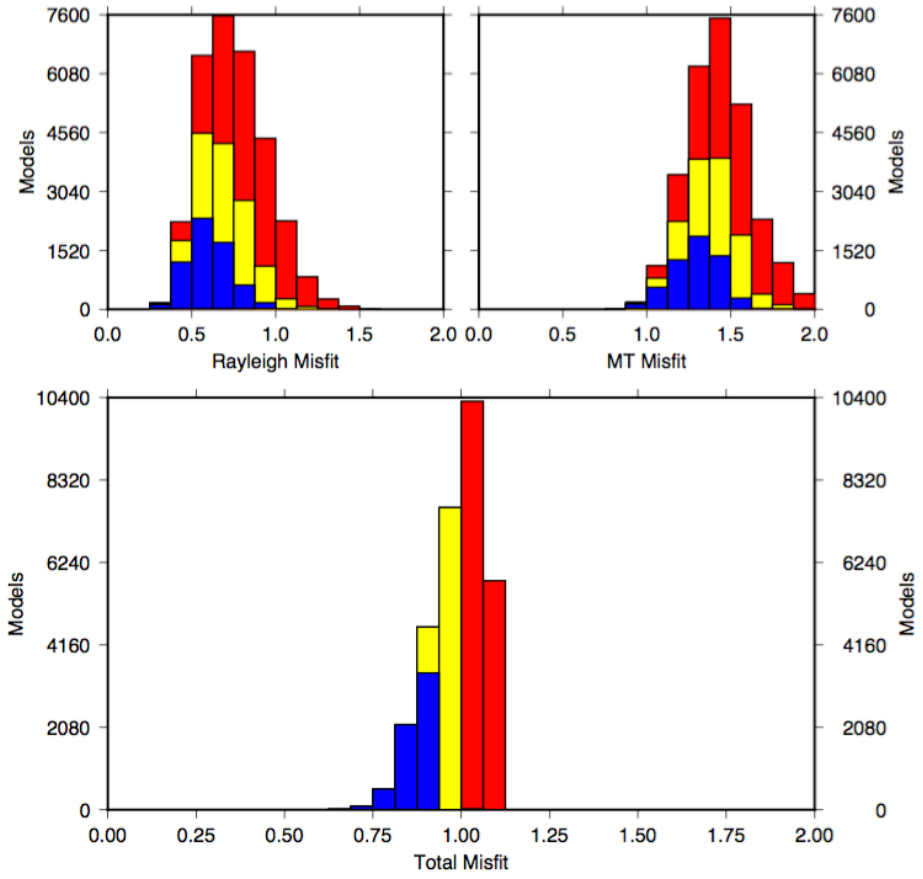

Figure S15.1: Histograms of the successful models. Red denotes models with a total nRMS<1.2, yellow models with an nRMS<1.00, and blue denotes models with an nRMS<0.90, as shown on the bottom plot. Note on the Rayleigh and MT misfit plots, that some models with total nRMS<1.00 fit the Rayleigh and/or MT data with nRMS>1.00

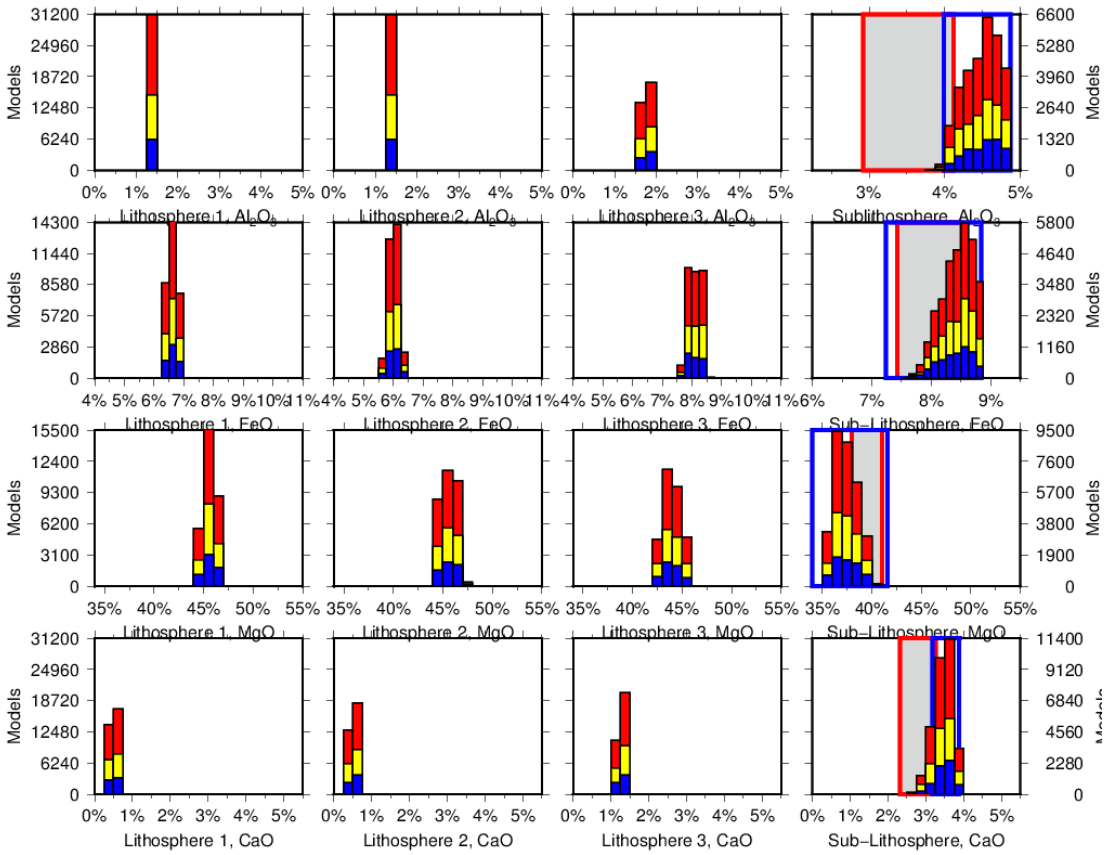

Figure S15.2: Posterior PDFs of the oxide chemistries of the three lithospheric layers (columns 1-3) and the sub-lithospheric mantle (column 4). The four rows are respectively percentages of Al_2O_3, FeO, MgO and CaO; the fifth oxide, SiO_3, is 100% minus the sum of all four. The two boxes on the SLM oxides are the Primitive Upper Mantle ranges for *McDonough and Sun* [1995] (blue boxes) and *Lyubetskaya and Korenaga* [2007] (grey shaded red boxes). Red denotes models that fit with a normalized summed RMS of <1.09, yellow denotes models with an nRMS < 1.00, and blue denotes models with an nRMS < 0.92.

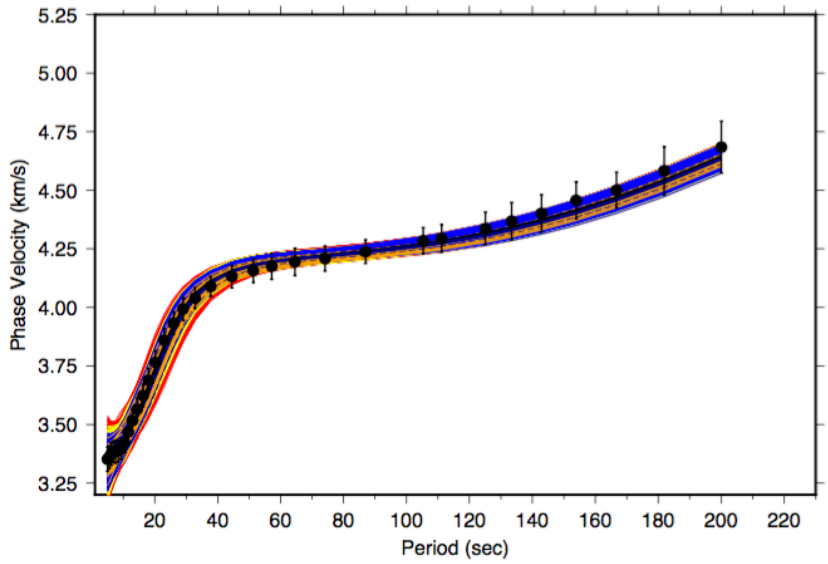

Figure S15.3: Fits of the models to the Rayleigh wave dispersion data (black circles with error bars). Red denotes models that fit with a normalized summed RMS of <1.09, yellow denotes models with an nRMS < 1.00, and blue denotes models with an nRMS , 0.92. Gold denotes those models that fit all four data types independently to an nRMS<1.

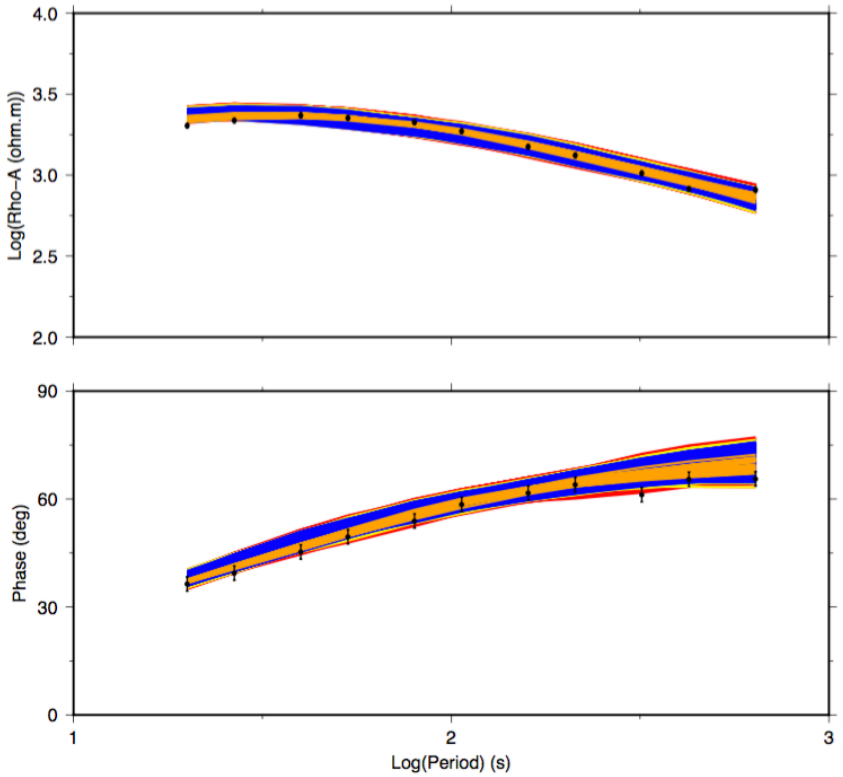

Figure S15.4: Fits of the models to the MT data (black circles with error bars). Red denotes models that fit with a normalized summed RMS of <1.09, yellow denotes models

with an nRMS < 1.00, and blue denotes models with an nRMS , 0.92. Gold denotes those models that fit all four data types independently to an nRMS<1.

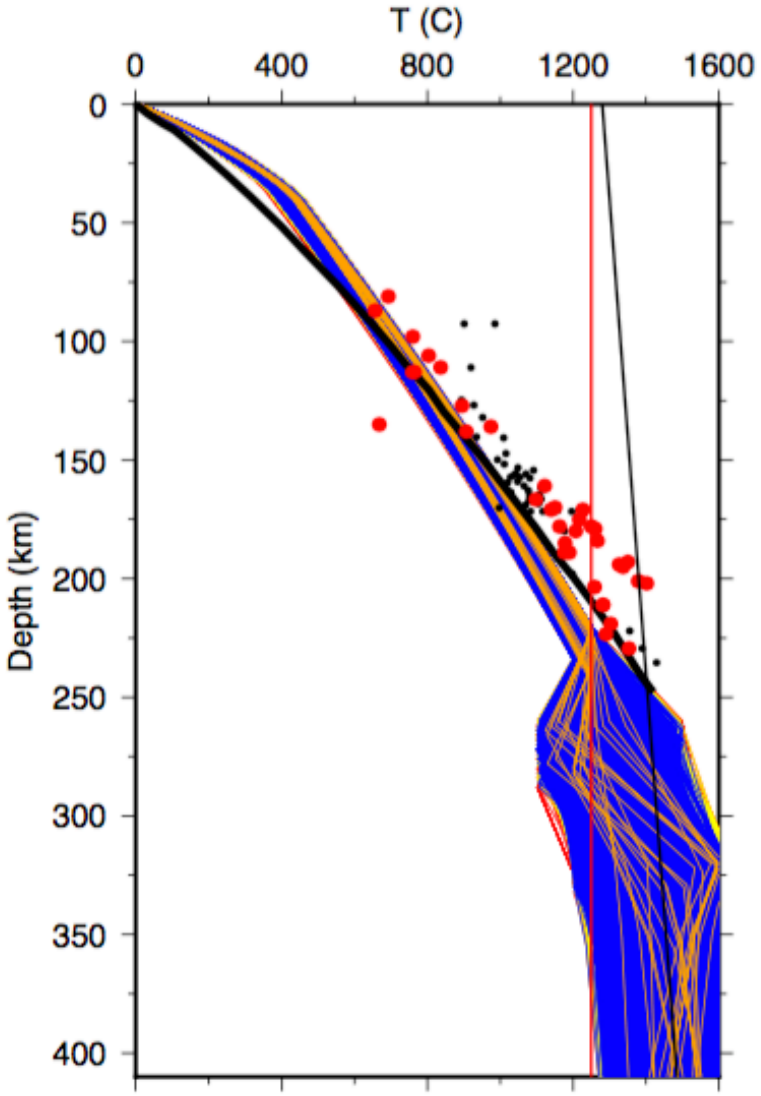

Figure S15.5: Geotherms for the successful models. Red denotes models that fit with a normalized summed RMS of <1.09, yellow denotes models with an nRMS < 1.00, and blue denotes models with an nRMS < 0.92. Gold denotes those models that fit all four data types independently to an nRMS<1. Also plotted on the figure is geotherm K2 (solid black line) of the Kaapvaal Craton derived by *Jones* [1988] based on the heat flow from granitic terranes, and the petrologically-derived P-T data based on petrological geothermometry of xenoliths from the Group I kimberlites on the Kaapvaal Craton [*Woodland and Koch*, 2003] (red for Jagersfontein, black for other kimberlite fields). Our models are hotter in the crust and uppermost mantle, and actually are closer to geotherm K1 of *Jones* [1988] (not shown) which was derived based on the higher heat flow on the Witwatersrand Basin, but have a lower gradient in the lithosphere and are cooler than the thermally-modeled geotherm or the P-T estimates.

References

Jones, M. Q. W. (1988), Heat flow in the Witwatersrand Basin and environs and its significance for the South African shield geotherm and lithosphere thickness, *Journal of Geophysical Research-Solid Earth and Planets*, *93*(B4), 3243-3260.
Kennett, B. L. N., E. R. Engdahl, and B. R. (1995), Constraints on seismic velocities in the Earth from travel times, *Geophysical Journal of the Royal Astronomical Society*, *122*, 108-124.
Lyubetskaya, T., and J. Korenaga (2007), Chemical composition of Earth's primitive mantle and its variance: 1. Method and results, *Journal of Geophysical Research-Solid Earth*, *112*(B03211).
McDonough, W. F., and S. S. Sun (1995), The composition of the Earth, *Chemical Geology*, *120*(3-4), 223-253.
McKenzie, D., and M. J. Bickle (1988), The volume and composition of melt generated by extension of the lithosphere, *Journal of Petrology*, *29*(3), 625-679.
McKenzie, D., and M. J. Bickle (1990), A eutectic parameterization of mantle melting, *Journal of Physics of the Earth*, *38*(6), 511-515.
Peslier, A. H., A. B. Woodland, D. R. Bell, and M. Lazarov (2010), Olivine water contents in the continental lithosphere and the longevity of cratons, *Nature*, *467*(7311), 78-81.
Woodland, A. B., and M. Koch (2003), Variation in oxygen fugacity with depth in the upper mantle beneath the Kaapvaal craton, Southern Africa, *Earth and Planetary Science Letters*, *214*(1-2), 295-310.